Direct structural evidence of protein redox regulation obtained by in-cell NMR

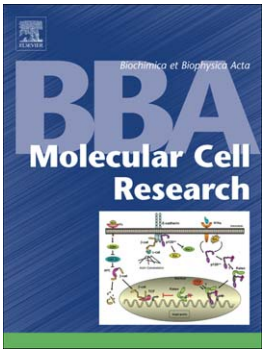

Direct structural evidence of protein redox regulation obtained by in-cell NMR

Eleonora Mercatelli, Letizia Barbieri, Enrico Luchinat, Lucia Banci

PII: S0167-4889(15)00393-6
DOI: doi: 10.1016/j.bbamcr.2015.11.009
Reference: BBAMCR 17720

To appear in: *BBA - Molecular Cell Research*

Received date: 7 October 2015
Revised date: 4 November 2015
Accepted date: 7 November 2015

Please cite this article as: Eleonora Mercatelli, Letizia Barbieri, Enrico Luchinat, Lucia Banci, Direct structural evidence of protein redox regulation obtained by in-cell NMR, *BBA - Molecular Cell Research* (2015), doi: 10.1016/j.bbamcr.2015.11.009

Direct structural evidence of protein redox regulation obtained by in-cell NMR

Eleonora Mercatelli[a], Letizia Barbieri[a,b], Enrico Luchinat[a,c], Lucia Banci[a,b,1]

[a]Magnetic Resonance Center - CERM, University of Florence, Via Luigi Sacconi 6, 50019 Sesto Fiorentino, Florence, Italy.

[b]Department of Chemistry, University of Florence, Via della Lastruccia 3, 50019 Sesto Fiorentino, Florence, Italy.

[c]Department of Biomedical, Clinical and Experimental Sciences, University of Florence, Viale Morgagni 50, 50134 Florence, Italy.

[1]To whom correspondence should be addressed. Telephone: +39 055 457 4273. Email: banci@cerm.unifi.it

Abstract

The redox properties of cellular environments are critical to many functional processes, and are strictly controlled in all living organisms. The glutathione-glutathione disulfide (GSH-GSSG) couple is the most abundant intracellular redox couple. A GSH redox potential can be calculated for each cellular compartment, which reflects the redox properties of that environment. This redox potential is often used to predict the redox state of a disulfide-containing protein, based on thermodynamic considerations. However, thiol-disulfide exchange reactions are often catalyzed by specific partners, and the distribution of the redox states of a protein may not correspond to the thermodynamic equilibrium with the GSH pool. Ideally, the protein redox state should be measured directly, bypassing the need to extrapolate from the GSH. Here, by in-cell NMR, we directly observe the redox state of three human proteins, Cox17, Mia40 and SOD1, in the cytoplasm of human and bacterial cells. We compare the observed distributions of redox states with those predicted by the GSH redox potential, and our results partially agree with the predictions. Discrepancies likely arise from the fact that the redox state of SOD1 is controlled by a specific partner, its copper chaperone (CCS), in a pathway which is not linked to the GSH redox potential. In principle, in-cell NMR allows determining whether redox proteins are at the equilibrium with GSH, or they are kinetically regulated.

Such approach does not need assumptions on the redox potential of the environment, and provides a way to characterize each redox-regulating pathway separately.

Keywords: in-cell NMR; glutathione; redox regulation; nuclear magnetic resonance; disulfide bond

1. Introduction

Living systems have developed a strict control of the redox cellular environment. In most prokaryotes and all eukaryotes, the most abundant redox couple in the cell is the glutathione-glutathione disulfide (GSH-GSSG) couple [1,2]. The redox potential of the glutathione pool (E'_{GSH}) in a given cellular compartment, which is dependent on the $[GSH]^2/[GSSG]$ ratio, is therefore a critical parameter to understand the redox properties of the environment [1,3]. Consequently, numerous methods have been developed to quantitatively measure the absolute and relative concentration of both GSH and GSSG, either by chemical assays on cell extracts [4,5] or, more recently, by using GSH-sensitive intracellular fluorescent probes [6–8]. These methods have contributed much to understand how the intracellular E'_{GSH} is influenced under physiological and oxidative stress conditions, and have shown that some cellular compartments have a less reducing environment with respect to the cytoplasm, such as the endoplasmic reticulum (ER) and the mitochondrial inter-membrane space (IMS) [3,5,9,10]. In principle, from the E'_{GSH} of the various cellular compartments, the redox state of disulfide-containing proteins can be predicted, provided that the midpoint reduction potential (E°') of each protein is known, and such capability has allowed a deeper understanding of the many redox-dependent mechanisms of protein maturation, such as the PDI-mediated folding in the ER and the disulfide-relay system of the mitochondrial IMS [3,11–13].

Despite these remarkable examples, sometimes glutathione alone is not sufficient to understand intracellular redox processes. In order for the difference (ΔE) between E°' of a protein and E'_{GSH} to act as a driving force for thiol-disulfide redox reactions, allowing the system to move towards the thermodynamic equilibrium (given by the Nernst equation), there needs to be a direct reaction between the protein and GSH/GSSG. In biological systems, this is usually not the case, as thiol-disulfide reactions would occur on timescales many orders of magnitude slower, if they were not catalyzed by specific enzymes [14,15]. Consequently, the actual protein redox states cannot always be inferred from E'_{GSH}, as they also depend on the kinetics of the

catalyzed reactions. In fact, it has been even suggested that under some circumstances the redox properties of an intracellular environment may not depend on E'_{GSH} at all [14,16]. Moreover, the measure of E'_{GSH} itself poses some challenges, as the result can vary considerably depending on which method is used [17,18].

Ideally, when studying redox-regulated pathways, the redox state of the proteins involved should be monitored directly inside the cells, thus bypassing all the assumptions required by the use of E'_{GSH}. For this purpose, Nuclear Magnetic Resonance applied to observe proteins in living cells (in-cell NMR) is a promising approach. In-cell NMR has been successfully applied to obtain atomic-level information on protein structure, dynamics and interactions in both bacterial and eukaryotic cells [19–22]. In particular, in-cell NMR can be applied to monitor protein maturation pathways involving the formation of one or more disulfide bonds [23–26]. NMR is extremely sensitive to changes in protein structure and dynamics, thus it easily detects the formation of disulfide bonds as they affect the protein structure and consequently the chemical shifts.

In this work, we report the direct observation of the redox state of three soluble proteins expressed in the cytoplasm of both human (HEK293T) and bacterial cells (*E. coli* BL21 and Origami B strains). By integrating the obtained data with previously reported findings, we determined the actual distributions of redox states of each protein in different cell types, and we compared them with those calculated from the reported E°' of the protein and cytoplasmic E'_{GSH} of each cell type. Due to the broad range of reported E'_{GSH} values, the redox state distributions predicted from the Nernst equation can change considerably. Despite this, our data is not always compatible with the range of E'_{GSH} values, suggesting that the observed proteins are not at the thermodynamic equilibrium with the environment. We also analyzed how the redox state distribution of the observed proteins changes in response of supplemented cofactors or increased levels of redox partners. In principle, with a more accurate estimate of E'_{GSH} in our experimental conditions, this method could be used to determine how far the steady-state distribution of redox sates of a protein is from the equilibrium with the E'_{GSH} of the environment in each cell type.

2. Materials and Methods

2.1. Gene cloning

cDNA encoding full-length human Cox17 (amino acids 1–63, GenBank: NP_005685) was amplified by PCR and cloned into the pHLsec [27] vector between EcoRI and XhoI restriction enzyme sites to generate the mammalian expression plasmid and into the pET16b plasmid between NdeI and XhoI restriction enzyme sites to generate the bacterial expression plasmid. cDNA encoding full-length human Mia40 (amino acids 1–142, GenBank: NP_001091972.1) was amplified by PCR and cloned into the pET21a between NdeI and XhoI restriction enzyme sites to generate the bacterial expression plasmid. All clones were verified by DNA sequencing. SOD1 in pET28a, pET21a and pHLsec, and Mia40, Grx1 and Trx1 in pHLsec were cloned as previously reported [23–25].

2.2. Human cell culture and transfection

HEK293T cells were maintained in DMEM (high glucose, D6546, Sigma) supplemented with L-glutamine, antibiotics (penicillin and streptomycin) and 10% FBS (Gibco) in uncoated 75 cm^2 plastic flasks and incubated at 310 K, 5% CO_2 in a humidified atmosphere.

HEK293T cells were transiently transfected with the pHLsec plasmid containing the gene of interest using polyethylenimine (PEI), as previously described [24]. Different DNA:PEI ratios were tested for maximizing protein expression (PEI was kept constant at 50 µg/flask), and an optimal ratio of 1:1 was used (50 µg/flask DNA, 50 µg/flask PEI). For co-expression of Cox17 and Grx1 or Cox17 and Trx1, cells were transfected with plasmids containing the constructs in different amounts and ratios. The ratios were chosen in order to obtain similar expression levels of Cox17, specifically 1.9:0.1:2 was used for Cox17:Grx1:PEI and 1.5:0.5:2 for Cox17:Trx1:PEI. To ensure complete activation of Trx1, sodium selenite was supplemented to the cell culture media to a final concentration of 100 nM, starting 24 h before transfection.

During protein expression, commercial DMEM medium was used to prepare unlabeled in-cell NMR samples; BioExpress6000 medium (CIL) was used for U-^{15}N labelling; for selective [^{15}N]cysteine labelling a reconstituted medium was prepared following the DMEM (Sigma) reported composition, in which [^{15}N]cysteine was added together with all the other unlabelled components. The expression media were supplemented with 2% FBS and antibiotics.

2.3. Western Blot analysis

Cox17 expression levels were determined on cell extracts by Western Blot analysis, by using a sample of purified Cox17 at increasing dilutions as a reference; Grx1 and Trx1 concentrations in the cell extracts were determined as above, by using samples of purified Grx1 and Trx1 as references. Cox17 was stained with a rabbit polyclonal anti-Cox17 antibody (Abcam: ab69611, diluted to 0.5 μg/ml); Grx1 with a rabbit polyclonal anti-glutaredoxin 1 antibody (Abcam: ab45953, 1.0 μg/ml); Trx1 with a rabbit polyclonal anti-thioredoxin/TRX antibody (Abcam: ab26320, 0.4 μg/ml). Goat anti-rabbit IgG (whole molecule)-peroxidase secondary antibody (Sigma: A0545) was used for detection, diluted at 1:80000.

2.4. Protein expression and purification

Pure Cox17 sample was produced following a previously described protocol [28]. Briefly, the pETG-30A vector containing the hCox17 gene was transformed in *E. coli* Origami B (DE3) cells (Novagen). Cells were induced with 0.5 mM IPTG for 16 h at 25 °C. Cox17 was purified by affinity chromatography using a nickel chelating HisTrap (GE Healthcare) column. After digestion with AcTEV protease (Invitrogen) O/N at 25 °C the protein was separated from the affinity tag in a HisTrap column. The sample buffer was then exchanged with 50 mM potassium phosphate, 0.5 mM EDTA, pH=7. Grx1 for reference in the WB analysis was produced as previously described [25]. Briefly, the pTH34 vector containing the human Grx1 gene was transformed in *E. coli* BL21(DE3) Gold competent cells. Cells were grown at 37 °C in minimal medium until O.D. 0.6 and then induced with 0.5 mM IPTG for 16 h at 25 °C. Grx1 was purified by affinity chromatography using a nickel chelating HisTrap (GE Healthcare) column. After digestion with AcTEV protease (Invitrogen) O/N at 25 °C the protein was separated from the affinity tag in a HisTrap column. The sample buffer was then exchanged with 50 mM potassium phosphate, 0.5 mM EDTA, pH=7. Pure Trx1 for WB analysis was prepared from HEK293T cells overexpressing Trx1 as previously described [25]. Cells were lysed in 20 mM potassium phosphate buffer (pH 7) and the cleared extract was incubated at 70°C for 4 min. After centrifugation (30 min at 16000 g), Trx1 was purified by anionic exchange chromatography using a HiTrap™ DEAE FF (Amersham Biosciences) column applying a linear gradient of potassium phosphate buffer (10 to 100 mM, pH 7).

2.5. In-cell NMR sample preparation (human cells)

HEK293T cells for in-cell NMR samples were collected as previously reported [24]. Briefly, cells from a 75 cm^2 flask were detached by trypsin treatment and suspended in one cell pellet volume of DMEM medium supplemented with 90 mM glucose, 70 mM HEPES buffer and 20% D_2O. The cell suspension was transferred to a 3 mm Shigemi tube; cells were spun down at the bottom of the tube. Cell viability before and after NMR experiments remained above 90%, as determined by trypan blue staining. Cleared cell lysates were prepared as follows: cells were suspended in one pellet volume of PBS buffer supplemented with 0.5 mM EDTA and 4-(2-aminoethyl)-benzenesulfonyl fluoride hydrochloride (AEBSF, Sigma) and lysed by freeze-thaw cycles with liquid N_2 and warm water. The cell lysate was centrifuged (60 min at 16000g, 4°C) and the cleared supernatant was recovered for NMR analysis in a 3 mm standard tube.

2.6. In-cell NMR sample preparation (bacterial cells)

U-^{15}N Samples for in-cell NMR in *E. Coli* cells were prepared as follows: a cell culture of BL21 (DE3) Gold (Agilent Technologies) or Origami B (DE3) (Novagen) transformed with the plasmid containing the gene of interest was grown overnight at 30°C in 35 mL of LB medium. After gentle centrifugation (3000 g) for 20 minutes, the cells were re-suspended in 50 mL of M9 minimal medium [M9 buffer (7 g/L K_2HPO_4, 3 g/L KH_2PO_4, 0.5 g/L NaCl, pH 7.4), 2 mM $MgSO_4$, 0.1 mM $CaCl_2$, 1 mg/L biotin, 1 mg/L thiamine, antibiotic] containing 1 g/L $(^{15}NH_4)_2SO_4$ and 3 g/L of unlabelled glucose to obtain an OD_{600} of ~1.6. After 10 min recovery time, overexpression was induced with 0.5 mM IPTG, and carried out at 30°C for 4 h. The cells were washed once with 50 mL of M9 buffer in order to remove nutrients, metal ions and any excreted by-product, and they were harvested through gentle centrifugation. The pellet was then re-suspended in M9 buffer until 500 µL of a ~50% v./v. cell slurry were obtained. 50 µL of D_2O were added, and the final volume was put in a 5 mm NMR tube. The cleared cell lysates for NMR experiments were prepared as follows: the cell pellet was re-suspended in an equal volume of M9 buffer and lysed by ultrasonication. The cell lysate was centrifuged (40 minutes at 18000 g, 4°C), the supernatant was collected and its volume was brought to 500 µL with M9 buffer; 50 µL of D_2O were added. The sampled was placed into a standard 5 mm tube for NMR analysis.

2.7. In-cell NMR experiments

NMR experiments on human cells and lysates were acquired at a 950 MHz Bruker Avance III spectrometer equipped with a CP TCI CryoProbe. NMR experiments on bacterial cells and lysates were acquired at a 900 MHz Bruker Avance spectrometer equipped with a TCI Cryoprobe. 1D ^{1}H and 2D ^{1}H-^{15}N SOFAST HMQC [29] spectra were acquired at 307 K. The total acquisition time for each cell sample was ~1 h. The supernatant of each cell sample was checked in the same experimental conditions to exclude the presence of any signal arising from protein leaked out of the cells. The same NMR spectra were also acquired on the cell lysates. The NMR spectra were processed with Bruker Topspin software. The 2D NMR spectra acquired on U-^{15}N labelled human cells and lysates were further processed by subtracting a spectrum of untransfected cells/cell lysate acquired in the same experimental conditions and identically processed, to eliminate the signals arising from partial ^{15}N labelling of other cellular components.

2.8. Analysis of the redox state distribution

The ratio of oxidized vs. total protein was calculated as follows: for Cox17, the ratio was obtained by integrating crosspeaks in the 2D NMR spectra corresponding to the oxidized and the reduced species (2D NMR spectra of [^{15}N]cysteine-labelled cells were used for human cells, of U-^{15}N labelled lysates for bacteria); for Mia40 in human cells, the values previously reported were used [25]; for Mia40 in bacteria, the 2D NMR spectra of the lysates were used; for SOD1 in human cells, the ratio was obtained by integrating crosspeaks in the 2D in-cell NMR spectra corresponding to the oxidized and the reduced species (from a U-^{15}N labelled sample for E,Zn-SOD1; from a [^{15}N]cysteine-labelled sample for Cu,Zn-SOD1); for SOD1 in bacteria, 2D NMR spectra of U-^{15}N labelled cells were used. The error bars were obtained by taking the standard deviation of the spectral noise as the error of the integrals, followed by error propagation.

2.9. Redox species plots

The redox species curves for each protein as a function of the GSH redox potential were calculated from the Nernst equation applied to the reaction between the oxidized protein and 2 GSH molecules:

$$P_{ox} + 2GSH \rightleftharpoons P_{red} + GSSG \qquad 1$$

where P_{ox} and P_{red} indicate the protein in the oxidized and reduced state, respectively. The corresponding Nernst equation at the equilibrium is:

$$0 = E^{\circ\prime}{}_P - E^{\circ\prime}{}_{GSH} - \frac{RT}{zF}\ln\frac{[GSSG][P_{red}]}{[GSH]^2[P_{ox}]} \qquad 2$$

where $E^{\circ\prime}{}_P$ is the protein midpoint potential at pH = 7; $E^{\circ\prime}{}_{GSH}$ is the reduction potential of GSH at pH = 7; R = 8.314 J K^{-1} mol^{-1}; T = 310 K; z = 2; F = 96485 C mol^{-1}. The GSH reduction potential (E'_{GSH}) in each cellular environment is given by:

$$E'_{GSH} = E^{\circ\prime}{}_{GSH} - \frac{RT}{zF}\ln\frac{[GSH]^2}{[GSSG]} \qquad 3$$

Combining eq. 3 with eq. 2 gives:

$$0 = E^{\circ\prime}{}_P - E'_{GSH} - \frac{RT}{zF}\ln\frac{[P_{red}]}{[P_{ox}]} \qquad 4$$

Which is rearranged to give the fraction of oxidized protein (ox. fraction) as a function of E'_{GSH}:

$$ox.fraction = \frac{[P_{ox}]}{[P_{ox}]+[P_{red}]} = \frac{1}{1+e^{-\frac{RT}{zF}(E'_{GSH}-E^{\circ\prime}{}_P)}} \qquad 5$$

The oxidized fraction vs. E'^{GSH} plots were obtained using the reported midpoint potentials for each protein (corrected for pH = 7.0): $E^{\circ\prime}{}_{Cox17} = -305$ mV[30]; $E^{\circ\prime}{}_{Mia40} \leq E^{\circ\prime}{}_{Cox17}$ [31]; $E^{\circ\prime}{}_{E,Zn\text{-}SOD1} = -320$ mV [32]; $E^{\circ\prime}{}_{Cu,Zn\text{-}SOD1} = -305$ mV [32,33]. In the case of Cox17 and Mia40 two disulfide bonds are formed, requiring the oxidation of four GSH molecules. However, the redox curve of Cox17 had been previously determined experimentally *in vitro*, and had been fitted with parameters compatible with the oxidation of two GSH molecules (i.e. the formation of one disulfide bond, see eq. 1) [30]. Therefore, eq. 5 was also used to calculate the redox curves of Cox17 and Mia40.

3. Results

3.1. Mitochondrial CHCH proteins

We have analyzed the folding and redox state of two small proteins of the mitochondrial IMS, human Cox17 and Mia40, in the cytoplasm of human and bacterial cells [28,31]. Like most mitochondrial proteins, Cox17 and Mia40 are synthesized in the cytoplasm, and have to translocate to the mitochondria [13,34]. Both proteins are constituted by a coiled-coil helix coiled-coil helix (CHCH) domain, consisting of two alpha helices stabilized through two structural disulfide bonds [35]. In order to reach the IMS, these small CHCH proteins can only cross the outer mitochondrial membrane in an unfolded state, therefore with the four cysteines of the CHCH motif reduced. ^{15}N-labelled Cox17 and Mia40 were overexpressed in the cytoplasm of human cells (E'_{GSH} ranging from –300 mV to –320 mV [36–39]), and the backbone amide signals of the folded CHCH domain were detected for both proteins (Fig. 1A,B), with their chemical shifts matching those of the *in vitro* NMR spectra of the folded, oxidized proteins [28,31]. This observation is further confirmed by the in-cell NMR spectra of [^{15}N]cysteine-labelled proteins (Fig. 1C,D). The ratio of folded Cox17 over total Cox17 was determined from the intensities of cysteine crosspeaks corresponding to the oxidized and reduced protein (Fig. 1D-F), while the ratio of folded Mia40 over total Mia40 was determined from the intensities of a set of crosspeaks in the in-cell NMR spectra of the ^{15}N-labelled protein (Fig. 1G-I). For Mia40, this method yielded results consistent with previous measurements [25]. This analysis revealed that in the human cytoplasm ~70% of Cox17 and ~75% of Mia40 are folded and therefore oxidized (Fig. 2A,B), and consequently unable to enter mitochondria. The values obtained were somewhat higher that those predicted from the Nernst equation (ranging between 25% and 60% oxidized over total protein) using the reported E'_{GSH} values. As we had previously shown [25], the folding state of Mia40 in the human cytoplasm is dependent on the levels of the cytoplasmic proteins thioredoxin 1 (Trx1) and glutaredoxin 1 (Grx1): when Grx1 or Trx1 were co-expressed with Mia40, the latter shifted towards the unfolded, reduced state as a function of Grx1/Trx1 levels (Fig. 2B). A similar, albeit moderate effect on the folding state of Cox17 was observed when Grx1 was co-expressed, while co-expression of Trx1 had a smaller effect (Fig. 1E,F, Fig. 2A and Fig. S1).

When Cox17 and Mia40 were expressed in *E. coli* BL21 cells (E'_{GSH} = –259 / –261 mV [40,41]) both proteins were mostly unfolded and in the reduced state, and no folded protein was detected in either intact cells or lysates despite the apparently less reducing environment (Fig. 2A,B and Fig. S2). Only when the Origami B strain of *E. coli* was used, which lacks the genes encoding glutathione reductase and thioredoxin

reductase, and is even less reducing (E'_{GSH} = –235 mV [41]), the folded conformation was observed again: ~45% of Cox17 was folded, and Mia40 was completely folded (estimated from the cell lysate due to severe signal broadening of the folded domain of both proteins in bacterial cells) (Fig. 2A,B and Fig. S3).

3.2. Superoxide dismutase 1 and its copper chaperone

Unlike Cox17 and Mia40, which need to be reduced in the cytoplasm in order to reach their functional compartment, the cytoplasmic enzyme superoxide dismutase 1 (SOD1) in its active form harbours an intramolecular disulfide bond. We have previously characterized the SOD1 maturation process both in bacterial and human cells [23,24,26]. SOD1 sequentially binds one zinc ion, dimerizes, and binds one copper ion per subunit with simultaneous formation of the disulfide bond. The copper binding step requires the interaction with a specific copper chaperone for SOD1 (CCS). CCS also catalyzes the formation of the SOD1 intramolecular disulfide bond through an intermolecular thiol-disulfide exchange reaction with its C-terminal unfolded domain [32,42]. When SOD1 is expressed in human cells it readily binds zinc and dimerizes, and the zinc-bound form is observed by in-cell NMR (E,Zn-SOD1, Fig. 3A,B). In these conditions ~85% of E,Zn-SOD1 is found in the reduced state, as the endogenous CCS is apparently not sufficient to allow copper binding and disulfide bond formation (Fig. 2C). If CCS is co-expressed with SOD1 at similar levels, disulfide formation is partial in defect of copper, but almost reaches completion if excess copper is supplemented (~80% oxidized SOD1), and the mature protein Cu,Zn-SOD1 is formed (Fig. 2C and 3C,D).

Zinc binding and dimerization of SOD1 are known to occur spontaneously in bacterial cells, and Cu,Zn-SOD1 is formed when bacteria are treated with excess copper after protein expression, without the need of co-expressed CCS [23,24]. In *E. coli* BL21 cells E,Zn-SOD1 was mostly observed in the reduced state, whereas Cu,Zn-SOD1 was partially oxidized (~60%, Fig. 2C and Fig. S4A,B). In *E. coli* Origami B cells E,Zn-SOD1 had already reached the oxidized state (~85%), and after copper supplementation fully oxidized Cu,Zn-SOD1 was observed (Fig. 2C and Fig. S4C,D).

4. Discussion

If a disulfide-containing protein is assumed to be at the equilibrium with the environment, the distribution of its redox states can be calculated from the difference between E°' of the protein and E'_{GSH} measured in the cellular compartment of interest, using the Nernst equation. When considering some uncertainty in the actual E'_{GSH} of the cytoplasm (as shown from the previously reported values), the redox state distribution of each observed protein can be expected to fall within a certain range (Fig. 2). In the case of Cox17 and Mia40 expressed in human cells, our data show that the redox states observed by in-cell NMR fall slightly out of the predicted range, towards the oxidized state (Fig. 2A,B). Interestingly, when the levels of redox-regulating proteins Grx1/Trx1 are increased, our data agree with the E'_{GSH} values previously reported, indicating that those proteins contribute to establish the thermodynamic equilibrium between Cox17/Mia40 and the GSH pool. Unlike for Cox17 and Mia40, the data obtained on SOD1 in human cells are not in agreement with the predicted redox state distributions: E,Zn-SOD1 is mostly reduced while Cu,Zn-SOD1 is mostly oxidized, while in both metallation states SOD1 is expected to populate both states (Fig. 2C). This discrepancy suggests that SOD1 never reaches the thermodynamic equilibrium with the GSH pool, and its redox state is determined by different factors, e.g. CCS. Indeed the interaction with CCS, which affected dramatically the redox state of SOD1, is known to catalyze the formation of SOD1 disulfide bond together with copper transfer [43], moving the final distribution of SOD1 redox states further away from the equilibrium with the GSH pool. These results suggest that the disulfide exchange between SOD1 and CCS is uncoupled from the glutathione pool, and that the redox pathway of CCS is not driven by the glutathione redox potential. On the contrary, the Grx1 pathway is expected to be dependent on the glutathione redox potential, as glutaredoxins catalyze thiol-disulfide exchange reactions between protein thiols and glutathione [44].

The data obtained in *E. coli* has a larger discrepancy from the predicted distribution of redox states (Fig. 2). Indeed, all three proteins are almost completely in the reduced state in *E. coli* BL21 cells, despite E'_{GSH} being less reducing compared to that of the mammalian cell cytoplasm. SOD1 in copper-treated BL21 cells is the only exception, as it is partially oxidized upon copper treatment. Only when the proteins are expressed in the Origami B strain, which is purposely designed to facilitate the folding of disulfide-containing proteins, all three proteins are observed in the oxidized state (either partially in the case Cox17, or completely in the case of Mia40 and SOD1). Given these discrepancies, one may speculate that in bacterial cells the distribution of oxidation states of our proteins does not reach the equilibrium with the GSH pool, and is mainly controlled

by the thioredoxin system (which is non-functional in the Origami B strain). Alternatively, our data could be compatible with a lower E'_{GSH} of *E. coli* cells (both BL21 and Origami B) than the reported values.

Lastly, discrepancies may also be introduced by macromolecular crowding, a property of the intracellular environment, which has been recently shown to affect the stability of protein folding [45–47]. If the change in redox state has a large effect on the folding state of a protein, the reduction potential measured *in vitro* may differ from the actual reduction potential in-cell. That would be especially true for Cox17 and Mia40, as the CHCH fold is strictly dependent on the disulfide bond formation, while the structure of SOD1 is not as much affected. While this effect may explain some discrepancies between the expected protein redox states and those actually observed by in-cell NMR, it does not justify the significant changes that occur in the same cellular environment when a redox partner is co-expressed at similar levels. Therefore, the observed changes are the result of specific redox-regulating processes.

5. Conclusions

The link between the intracellular glutathione and the redox state of the cell is an established property of living organisms. However, analysis at the molecular level reveals that the oxidation state of disulfide-containing proteins cannot be always predicted from the glutathione redox potential of the cellular compartment. By in-cell NMR analysis, we observed the redox state of three human proteins in the cytoplasm of human and bacterial cells. By obtaining direct information on the conformational properties of each protein in different redox states, we could directly obtain the distribution of redox states, which was then compared to the one predicted by assuming the thermodynamic equilibrium with GSH. In human cells, co-expression of redox-regulating protein partners altered the distribution of redox states. In bacterial cells (BL21) the proteins were mostly reduced, despite the less reducing cellular environment, while in the absence of the disulfide reduction pathways (in Origami B cells) the oxidized state of each protein was observed. Our results show that in-cell NMR is a suitable method to directly observe the redox state of a soluble disulfide-containing protein, and suggest that the oxidation state of some proteins is controlled by a specific pathway, which may not be linked to the GSH pool. Understanding such specific redox pathways

would require focussing on the interactions between the various partners (e.g. SOD1 and CCS) irrespective of the GSH pool, similarly to how kinase signalling cascades are studied.

Author contribution

Lu.B., Le.B. and E.L. conceived the work; Le.B., E.L. and E.M. designed the experiments; Le.B and E.M. cloned the genes, produced the in-cell NMR samples and performed the Western Blot analysis; E.L. performed the in-cell NMR experiments and analyzed the data; Lu.B., Le.B., E.L. and E.M. wrote the manuscript.

Acknowledgements

This work has been supported by "MEDINTECH: Tecnologie convergenti per aumentare la sicurezza e l'efficacia di farmaci e vaccini" and by Instruct, part of the European Strategy Forum on Research Infrastructures (ESFRI) and supported by national member subscriptions. Specifically, we thank the EU ESFRI Instruct Core Centre CERM-Italy.

Figure Legends

Fig. 1. In-cell NMR spectra of human cells expressing Cox17 and Mia40. (A-C) ^{1}H-^{15}N SOFAST-HMQC spectra of human cells expressing (A) [U-^{15}N]-labelled Cox17, (B) [U-^{15}N]-labelled Mia40, (C) [^{15}N]cysteine-labelled Mia40. (D-F) ^{1}H-^{15}N SOFAST-HMQC spectra of human cells expressing [^{15}N]cysteine-labelled Cox17 either alone (D) or in presence of increased levels of Grx1 (E) and Trx1 (F). (G-I) Selected region of ^{1}H-^{15}N SOFAST-HMQC spectra of human cells expressing [U-^{15}N]-labelled Mia40 either alone (G) or in presence of increased levels of Grx1 (H) and Trx1 (I). In (C-F), the amide crosspeaks corresponding to the cysteine residues in the oxidized, folded conformation are indicated. For Cox17, the crosspeak corresponding to a cysteine of the reduced conformation [C(red)] is indicated. In (G-I), the amide crosspeaks used to determine the redox state distribution are indicated.

Fig. 2. Protein redox state distributions measured by NMR in different cellular environments. Fraction of oxidized Cox17 (A), Mia40 (B) and SOD1 (C), experimentally measured through in-cell NMR in human HEK293T, *E. coli* BL21 and *E. coli* Origami B cells, plotted against the redox potential of the cytoplasmic glutathione pool reported for each cell type (E'_{GSH}, range shown as grey area, single values as dot-dashed lines). The oxidized fractions of Cox17 and Mia40 alone are shown as black squares, in presence of overexpressed Grx1 and Trx1 as black circles and triangles, respectively. E,Zn-SOD1 fractions are shown as red squares; Cu,Zn-SOD1 fractions as blue squares. Error bars are calculated from standard errors. The curves represent the predicted fraction of oxidized protein calculated from the Nernst equation for Cox17 (black), Mia40 (black), E,Zn-SOD1 (red) and Cu,Zn-SOD1 (blue).

Fig. 3. In-cell NMR spectra of human cells expressing SOD1. (A) ^{1}H-^{15}N SOFAST-HMQC spectrum of human cells expressing [U-^{15}N]-labelled SOD1 in presence of excess zinc, corresponding to the zinc-bound protein (E,Zn-SOD1); (B) detail of the NMR spectrum (A) with lower contour levels showing the crosspeaks arising from the Asn53 HNδ1, HNδ2 of E,Zn-SOD1^{SS} (ox) and E,Zn-SOD1^{SH} (red); (C) ^{1}H-^{15}N SOFAST-

HMQC spectrum of human cells expressing [^{15}N]cysteine-labelled SOD1 in presence of excess zinc and copper, and increased levels of CCS, in which Cu,Zn-SOD1 is observed; (D) detail of the NMR spectrum (E) with lower contour levels showing the crosspeaks arising from Cys146 of Cu,Zn-SOD1^{SS} (ox) and Cu,Zn-SOD1^{SH} (red).

References

1. Schafer FQ, Buettner GR (2001) Redox environment of the cell as viewed through the redox state of the glutathione disulfide/glutathione couple. *Free Radic Biol Med* **30**: 1191–1212.
2. Owen JB, Butterfield DA (2010) Measurement of oxidized/reduced glutathione ratio. *Methods Mol Biol Clifton NJ* **648**: 269–277.
3. Hwang C, Sinskey AJ, Lodish HF (1992) Oxidized redox state of glutathione in the endoplasmic reticulum. *Science* **257**: 1496–1502.
4. Kirlin WG, Cai J, Thompson SA, Diaz D, Kavanagh TJ, Jones DP (1999) Glutathione redox potential in response to differentiation and enzyme inducers. *Free Radic Biol Med* **27**: 1208–1218.
5. Dixon BM, Heath S-HD, Kim R, Suh JH, Hagen TM (2008) Assessment of endoplasmic reticulum glutathione redox status is confounded by extensive ex vivo oxidation. *Antioxid Redox Signal* **10**: 963–972.
6. Østergaard H, Tachibana C, Winther JR (2004) Monitoring disulfide bond formation in the eukaryotic cytosol. *J Cell Biol* **166**: 337–345.
7. Gutscher M, Pauleau A-L, Marty L, Brach T, Wabnitz GH, Samstag Y, Meyer AJ, Dick TP (2008) Real-time imaging of the intracellular glutathione redox potential. *Nat Methods* **5**: 553–559.
8. Morgan B, Sobotta MC, Dick TP (2011) Measuring E(GSH) and H2O2 with roGFP2-based redox probes. *Free Radic Biol Med* **51**: 1943–1951.
9. Hu J, Dong L, Outten CE (2008) The Redox Environment in the Mitochondrial Intermembrane Space Is Maintained Separately from the Cytosol and Matrix. *J Biol Chem* **283**: 29126–29134.
10. Kojer K, Bien M, Gangel H, Morgan B, Dick TP, Riemer J (2012) Glutathione redox potential in the mitochondrial intermembrane space is linked to the cytosol and impacts the Mia40 redox state. *EMBO J* **31**: 3169–3182.
11. Hudson DA, Gannon SA, Thorpe C (2015) Oxidative protein folding: from thiol-disulfide exchange reactions to the redox poise of the endoplasmic reticulum. *Free Radic Biol Med* **80**: 171–182.
12. Lu H, Allen S, Wardleworth L, Savory P, Tokatlidis K (2004) Functional TIM10 chaperone assembly is redox-regulated in vivo. *J Biol Chem* **279**: 18952–18958.
13. Mesecke N, Terziyska N, Kozany C, Baumann F, Neupert W, Hell K, Herrmann JM (2005) A disulfide relay system in the intermembrane space of mitochondria that mediates protein import. *Cell* **121**: 1059–1069.
14. Flohé L (2013) The fairytale of the GSSG/GSH redox potential. *Biochim Biophys Acta* **1830**: 3139–3142.
15. Berndt C, Lillig CH, Flohé L (2014) Redox regulation by glutathione needs enzymes. *Front Pharmacol* **5**: 168.
16. Morgan B (2014) Reassessing cellular glutathione homoeostasis: novel insights revealed by genetically encoded redox probes. *Biochem Soc Trans* **42**: 979–984.
17. Birk J, Meyer M, Aller I, Hansen HG, Odermatt A, Dick TP, Meyer AJ, Appenzeller-Herzog C (2013) Endoplasmic reticulum: reduced and oxidized glutathione revisited. *J Cell Sci* **126**: 1604–1617.
18. Morgan B, Ezeriņa D, Amoako TNE, Riemer J, Seedorf M, Dick TP (2013) Multiple glutathione disulfide removal pathways mediate cytosolic redox homeostasis. *Nat Chem Biol* **9**: 119–125.
19. Freedberg DI, Selenko P (2014) Live cell NMR. *Annu Rev Biophys* **43**: 171–192.
20. Hänsel R, Luh LM, Corbeski I, Trantirek L, Dötsch V (2014) In-cell NMR and EPR spectroscopy of biomacromolecules. *Angew Chem Int Ed Engl* **53**: 10300–10314.
21. Smith AE, Zhang Z, Pielak GJ, Li C (2015) NMR studies of protein folding and binding in cells and cell-like environments. *Curr Opin Struct Biol* **30**: 7–16.

22. Barbieri L, Luchinat E, Banci L (2015) Protein interaction patterns in different cellular environments are revealed by in-cell NMR. *Sci Rep* **5**: 14456.
23. Banci L, Barbieri L, Bertini I, Cantini F, Luchinat E (2011) In-cell NMR in E. coli to monitor maturation steps of hSOD1. *PloS One* **6**: e23561.
24. Banci L, Barbieri L, Bertini I, Luchinat E, Secci E, Zhao Y, Aricescu AR (2013) Atomic-resolution monitoring of protein maturation in live human cells by NMR. *Nat Chem Biol* **9**: 297–299.
25. Banci L, Barbieri L, Luchinat E, Secci E (2013) Visualization of redox-controlled protein fold in living cells. *Chem Biol* **20**: 747–752.
26. Luchinat E, Barbieri L, Rubino JT, Kozyreva T, Cantini F, Banci L (2014) In-cell NMR reveals potential precursor of toxic species from SOD1 fALS mutants. *Nat Commun* **5**: 5502.
27. Aricescu AR, Lu W, Jones EY (2006) A time- and cost-efficient system for high-level protein production in mammalian cells. *Acta Crystallogr D Biol Crystallogr* **62**: 1243–1250.
28. Banci L, Bertini I, Ciofi-Baffoni S, Janicka A, Martinelli M, Kozlowski H, Palumaa P (2008) A structural-dynamical characterization of human Cox17. *J Biol Chem* **283**: 7912–7920.
29. Schanda P, Brutscher B (2005) Very fast two-dimensional NMR spectroscopy for real-time investigation of dynamic events in proteins on the time scale of seconds. *J Am Chem Soc* **127**: 8014–8015.
30. Voronova A, Meyer-Klaucke W, Meyer T, Rompel A, Krebs B, Kazantseva J, Sillard R, Palumaa P (2007) Oxidative switches in functioning of mammalian copper chaperone Cox17. *Biochem J* **408**: 139–148.
31. Banci L, Bertini I, Cefaro C, Ciofi-Baffoni S, Gallo A, Martinelli M, Sideris DP, Katrakili N, Tokatlidis K (2009) MIA40 is an oxidoreductase that catalyzes oxidative protein folding in mitochondria. *Nat Struct Mol Biol* **16**: 198–206.
32. Banci L, Bertini I, Cantini F, Kozyreva T, Massagni C, Palumaa P, Rubino JT, Zovo K (2012) Human superoxide dismutase 1 (hSOD1) maturation through interaction with human copper chaperone for SOD1 (hCCS). *Proc Natl Acad Sci U S A* **109**: 13555–13560.
33. Bouldin SD, Darch MA, Hart PJ, Outten CE (2012) Redox properties of the disulfide bond of human Cu,Zn superoxide dismutase and the effects of human glutaredoxin 1. *Biochem J* **446**: 59–67.
34. Neupert W, Herrmann JM (2007) Translocation of proteins into mitochondria. *Annu Rev Biochem* **76**: 723–749.
35. Banci L, Bertini I, Ciofi-Baffoni S, Tokatlidis K (2009) The coiled coil-helix-coiled coil-helix proteins may be redox proteins. *FEBS Lett* **583**: 1699–1702.
36. Dooley CT, Dore TM, Hanson GT, Jackson WC, Remington SJ, Tsien RY (2004) Imaging dynamic redox changes in mammalian cells with green fluorescent protein indicators. *J Biol Chem* **279**: 22284–22293.
37. Schwarzer C, Illek B, Suh JH, Remington SJ, Fischer H, Machen TE (2007) Organelle redox of CF and CFTR-corrected airway epithelia. *Free Radic Biol Med* **43**: 300–316.
38. Meyer AJ, Dick TP (2010) Fluorescent protein-based redox probes. *Antioxid Redox Signal* **13**: 621–650.
39. Schwarzländer M, Dick TP, Meye AJ, Morgan B (2015) Dissecting Redox Biology using Fluorescent Protein Sensors. *Antioxid Redox Signal*.
40. Ostergaard H, Henriksen A, Hansen FG, Winther JR (2001) Shedding light on disulfide bond formation: engineering a redox switch in green fluorescent protein. *EMBO J* **20**: 5853–5862.
41. Zhang W, Zheng W, Mao M, Yang Y (2014) Highly efficient folding of multi-disulfide proteins in superoxidizing Escherichia coli cytoplasm. *Biotechnol Bioeng* **111**: 2520–2527.
42. Furukawa Y, Torres AS, O'Halloran TV (2004) Oxygen-induced maturation of SOD1: a key role for disulfide formation by the copper chaperone CCS. *EMBO J* **23**: 2872–2881.
43. Carroll MC, Girouard JB, Ulloa JL, Subramaniam JR, Wong PC, Valentine JS, Culotta VC (2004) Mechanisms for activating Cu- and Zn-containing superoxide dismutase in the absence of the CCS Cu chaperone. *Proc Natl Acad Sci U S A* **101**: 5964–5969.
44. Fernandes AP, Holmgren A (2004) Glutaredoxins: glutathione-dependent redox enzymes with functions far beyond a simple thioredoxin backup system. *Antioxid Redox Signal* **6**: 63–74.
45. Monteith WB, Pielak GJ (2014) Residue level quantification of protein stability in living cells. *Proc Natl Acad Sci U S A* **111**: 11335–11340.
46. Monteith WB, Cohen RD, Smith AE, Guzman-Cisneros E, Pielak GJ (2015) Quinary structure modulates protein stability in cells. *Proc Natl Acad Sci U S A* **112**: 1739–1742.

47. Majumder S, Xue J, DeMott CM, Reverdatto S, Burz DS, Shekhtman A (2015) Probing protein quinary interactions by in-cell nuclear magnetic resonance spectroscopy. *Biochemistry (Mosc)* **54**: 2727–2738.

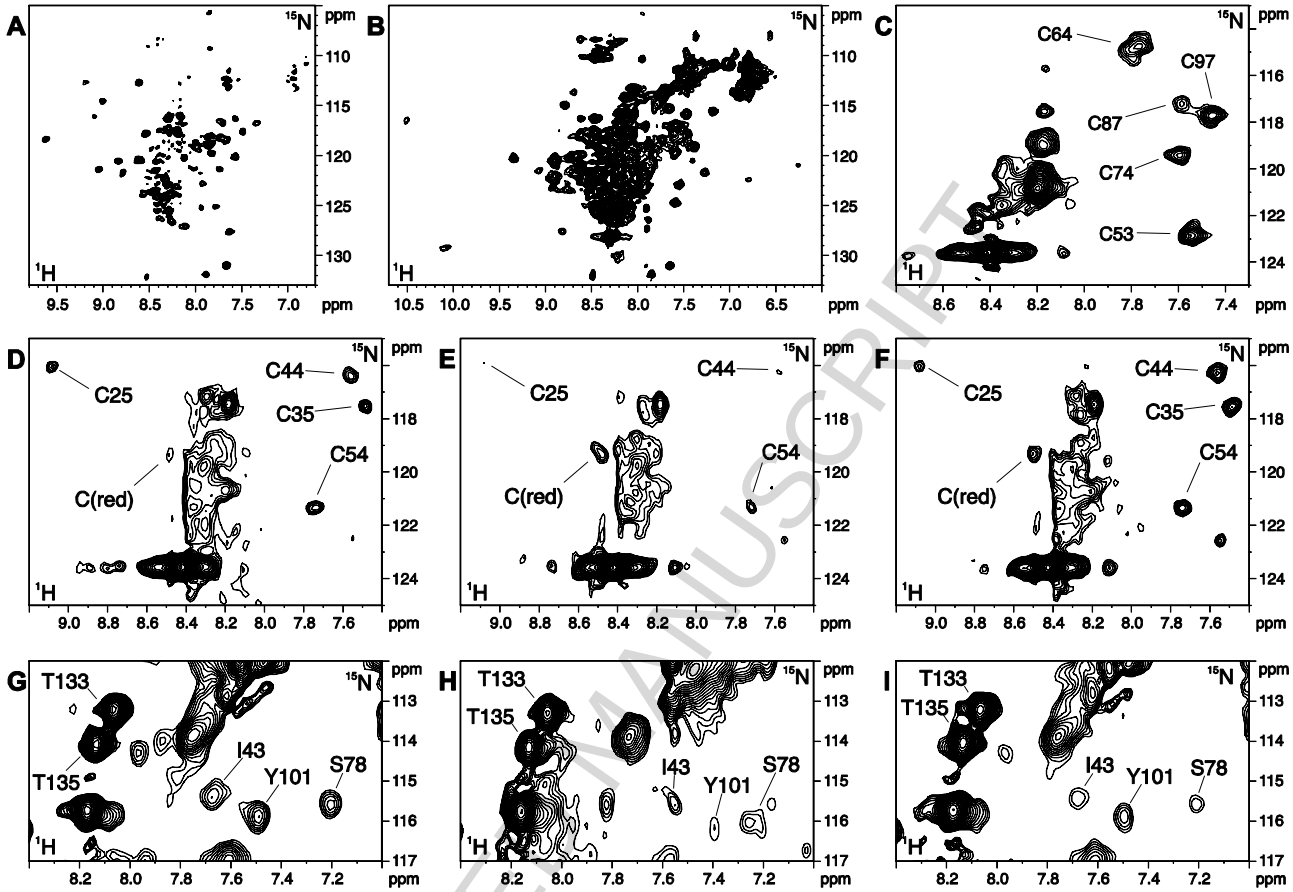

Figure 1

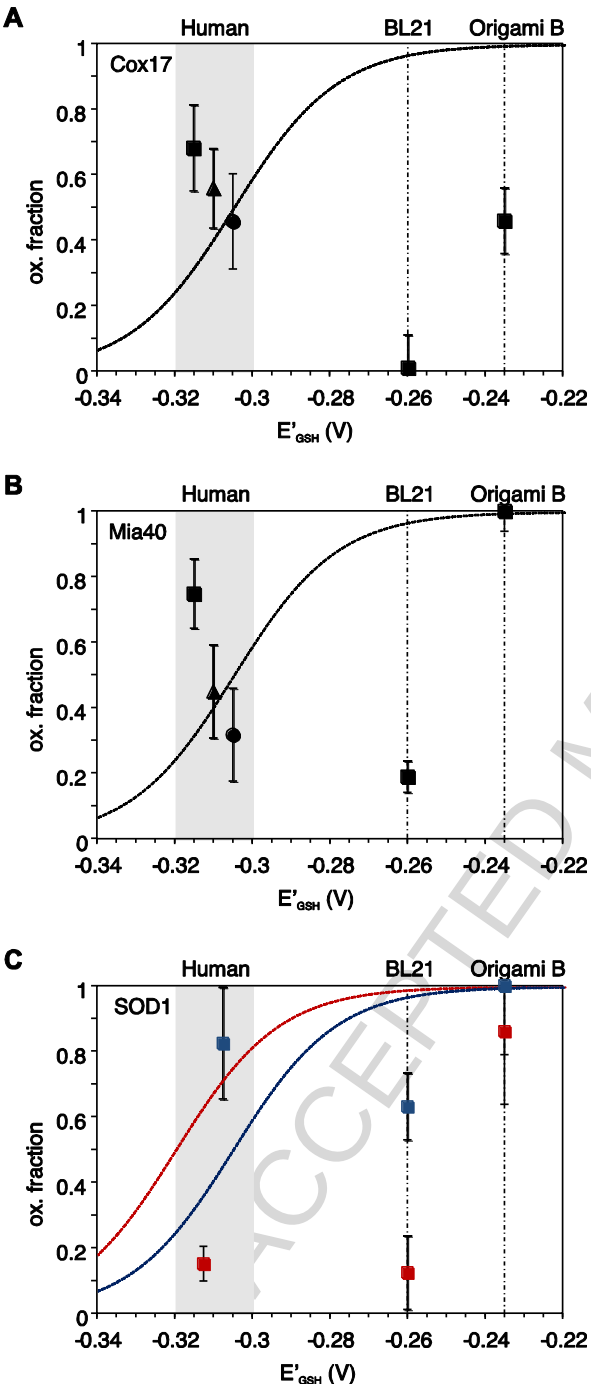

Figure 2

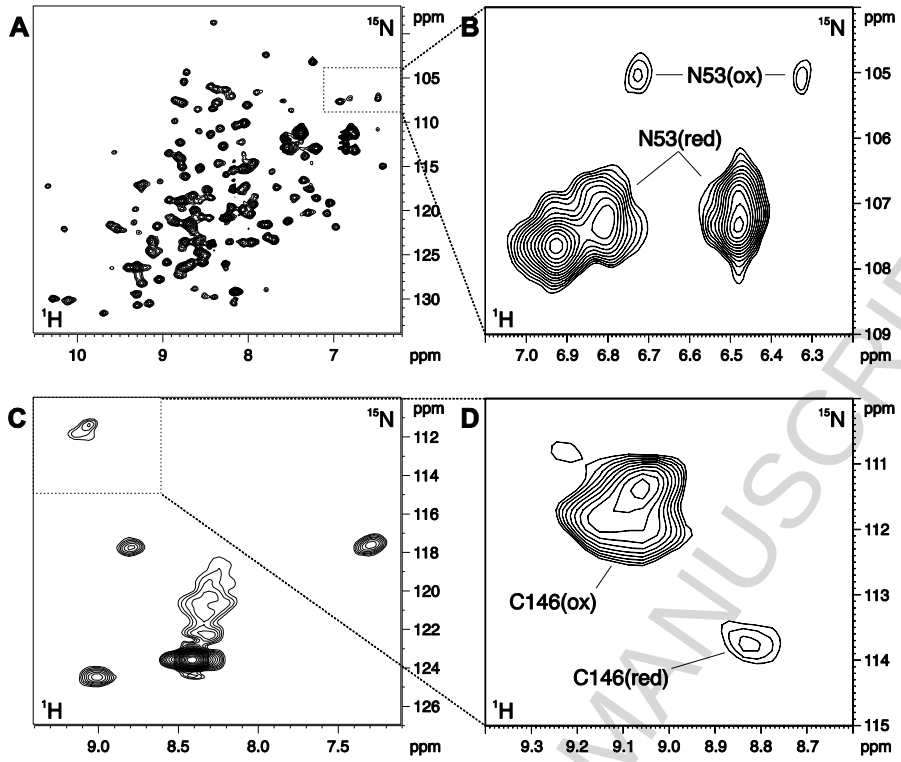

Figure 3

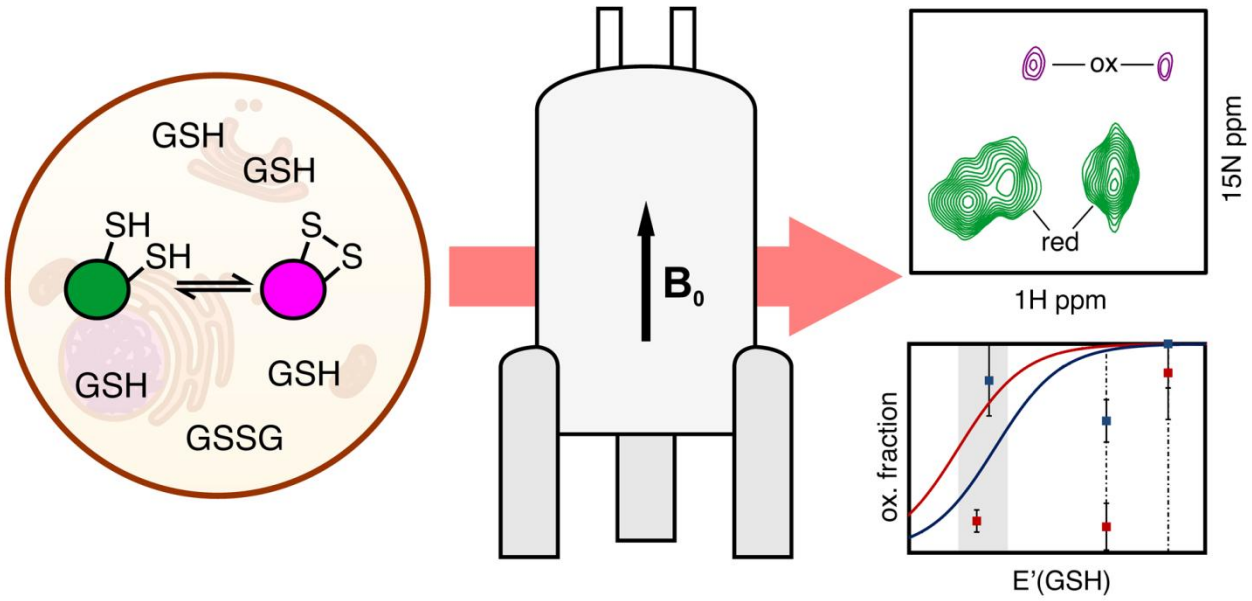

Graphical abstract

Highlights

- Protein redox state distributions can be measured directly in living cells by NMR.
- Some proteins do not reach the equilibrium with the intracellular glutathione pool.
- Non-equilibrium distributions indicate kinetic regulation by specific partners.